Polymer Chemistry

ROYAL SOCIETY OF CHEMISTRY

PAPER

View Article Online
View Journal | View Issue

Cite this: *Polym. Chem.*, 2024, **15**, 4244

Versatile poly(*N*-vinylcaprolactam)-*grafted*-hydroxypropyl cellulose polymers with tailored thermo- and pH-responsive properties *via* sustainable organocatalyzed atom transfer radical polymerization

Muhammad Asif Iqbal,[a] Asif Mahmood,[b] Waheed Al-Masry,[b] Chan Ho Park,[c] Sadaf Ul Hassan*[d] and Toheed Akhter *[c]

Received 25th August 2024,
Accepted 20th September 2024

DOI: 10.1039/d4py00931b

rsc.li/polymers

This study explores the synthesis of dual pH- and thermo-responsive poly(*N*-vinylcaprolactam)-*grafted*-hydroxypropyl cellulose (PNVCL-*g*-HPC) polymers *via* visible-light-driven, metal-free organocatalyzed atom transfer radical polymerization (O-ATRP). Three distinct PNVCL-*g*-HPC polymers were prepared with controlled molecular weights and narrow dispersity indexes by grafting PNVCL chains onto a cellulose-based macroinitiator. The polymerization was facilitated by 1,2,3,5-tetrakis(carbazol-9-yl)-4,6-dicyanobenzene, a photoredox catalyst that effectively uses visible light to start the polymerization. The resulting polymers were characterized using FT-IR spectroscopy, NMR spectroscopy, GPC, and TGA. By analyzing the transmittance of the PNVCL-*g*-HPC polymers as a function of temperature over a range of pH values (3–12), the lower critical solution temperature (LCST) of the polymers was determined. We successfully tuned the LCST of these polymers to a physiological range (25–38 °C) by adjusting the HPC and PNVCL monomer ratios. Notably, the HNC-18 polymer exhibited an LCST of approximately 37.2 °C, making it suitable for biological applications. These polymers, with adjustable LCSTs, hold promise for diverse applications in electronics, biosensors, pharmaceuticals, biomedical fields, and drug delivery systems.

1. Introduction

The capacity of stimuli-responsive polymers to undergo precise and regulated changes in response to environmental variations has attracted a lot of attention in recent years.[1] These materials can reversibly change their properties when subjected to external factors such as temperature, pH, light, and electric or magnetic fields.[2] The versatility and adaptability of stimuli-responsive polymers provide substantial benefits across a range of industries, notably in cosmetics and pharmaceuticals.[3] With increasing awareness about sustainability and a shift towards vegetarianism, there is a growing interest in developing cellulose-based stimuli-responsive polymers.[2–4]

Hydroxypropyl cellulose (HPC) is derived from the natural polysaccharide cellulose by introducing hydroxypropyl groups, which replace certain hydroxyl groups of cellulose, thereby forming hydrophobic propylene oxide groups.[5] It is highly effective as emulsifiers in cosmetic formulations and as flocculants in pharmaceutical applications. As a result, HPC has been investigated as a primary backbone for thermoresponsive graft copolymers in various fields.[4,6–8] However, the utility of HPC as a vital biomaterial is limited by its lower critical solution temperature (LCST) of 40 to 45 °C. This LCST range poses challenges for applications within the physiological temperature range of 25 to 38 °C, despite the possibility of altering the LCST through pH adjustments or salt additions.[8–11] Another approach to modify the LCST of HPC involves grafting it with different monomers, which can either raise or lower the LCST based on the specific reaction conditions. This modification enables HPC to operate within the physiological temperature range, enhancing its potential as a thermoresponsive platform.[12]

Poly(*N*-vinylcaprolactam) (PNVCL), a well-studied thermoresponsive polymer, has LCST between 25 and 50 °C. Generally, PNVCL shows its LCST very close to physiological temperature, which makes it a useful material for biomedical applications.[13–15] The molecular weight of the polymer, the

[a]*Department of Chemistry, School of Science, University of Management and Technology, C-II, Johar Town, 54770 Lahore, Pakistan*
[b]*Department of Chemical Engineering, College of Engineering, King Saud University, Riyadh, 11421, Saudi Arabia*
[c]*Department of Chemical and Biological Engineering, Gachon University, Seongnam, 13120, Republic of Korea. E-mail: toheed@gachon.ac.kr*
[d]*Department of Chemistry, COMSATS University Islamabad, Lahore Campus, Lahore, Defence Road, Off Raiwind Road, Lahore 54000, Pakistan. E-mail: sadafulhassan@cuilahore.edu.pk*

concentration of the polymer solution, and the existence of any additives can all affect the precise LCST. Additionally, for copolymers, LCST is also dependent on the chemical composition.[16,17] When synthesizing PNVCL, precise control over the dispersity index and molecular weight is essential since these parameters influence its LCST, which is essential for its usefulness in a variety of applications. The combination of biocompatibility, molecular interactions, and minimal toxicity makes PNVCL a promising material for numerous biomedical applications. Polymers containing PNVCL segments are particularly noteworthy for their potential in biomedical and pharmaceutical fields due to their biodegradability and biocompatibility.[15,18] As a result, PNVCL is an excellent choice for grafting onto HPC to adjust its LCST.

Grafting polymers onto a cellulose backbone can be carried out through a variety of techniques, such as atom transfer radical polymerization (ATRP), ring-opening polymerization, nitroxide-mediated polymerization (NMP), free radical polymerization, reversible deactivation radical polymerization (RDRP), and ring-opening polymerization.[19–21] Among these, ATRP is renowned for its ability to produce cellulose-based graft polymers with precise and well-defined structures.[5,22,23]

However, a major concern with ATRP, like other chemical processes, is the presence of transition metals in the final products, which can have significant environmental impacts if not properly managed. This issue has prompted the development of more environmentally friendly alternatives, such as metal-free organic photoredox catalysts and organocatalyzed polymerizations.[24] Contamination of synthesized polymers with transition metals poses a significant public health risk if they are not thoroughly removed during purification. Even in low concentrations, these metals can disrupt various biological processes in the human body, such as oxidation, protein activation, and metabolic regulation.[25–27]

To mitigate the issues associated with conventional ATRP, sustainable and environmentally friendly alternatives like visible light-mediated, metal-free organocatalyzed ATRP (O-ATRP) can be employed for the synthesis of biocompatible and thermoresponsive polymers, especially those with LCST in the physiological temperature range. O-ATRP effectively addresses polymer toxicity concerns and is a cost-efficient method for producing polymers with a low dispersity index ($Đ$), controlled chain-end functionalities, and well-defined architectures which is essential for fine-tuning the LCST in PNVCL-based polymers.

This method is especially advantageous for producing polymers with LCST values within the physiological range, making them highly desirable for biomedical applications.[5] Furthermore, O-ATRP can be considered a green synthetic process by utilizing visible light from natural daylight or energy-efficient LEDs to activate the organic photoredox catalyst. The use of organic photoredox catalysts in place of metal-based catalysts in ATRP method ensures a cleaner and more sustainable approach to polymer synthesis.[28]

Matyjaszewski *et al.* were pioneers in demonstrating the effectiveness of phenyl phenothiazine and related organic analogs in catalyzing the O-ATRP process.[26] Building on this foundation, Miyake *et al.* advanced the field by developing various organic photoredox catalysts for O-ATRP.[29] In our own research, we contributed to the field by establishing a design principle for creating diverse organic photoredox catalysts.[24] Following this approach, we selected 1,2,3,5-tetrakis(carbazol-9-yl)-4,6-dicyanobenzene (4CzIPN) as the organic photoredox catalyst for O-ATRP in our subsequent study, where it was used to synthesize thermoresponsive polymers.[5]

In this investigation, we developed cellulose-based PNVCL-*g*-HPC polymers with dual-stimuli responsiveness using the O-ATRP technique. We synthesized three distinct polymers with varying molar ratios of HPC to *N*-vinylcaprolactam (NVCL), designated as HNC-06, HNC-12, and HNC-18. Initially, 2-bromopropionyl bromide and HPC were reacted to prepare a macroinitiator. This macroinitiator then underwent O-ATRP with NVCL, facilitated by blue light irradiation using 4CzIPN as a catalyst. To our knowledge, this represents the first synthesis of such dual-stimuli-responsive PNVCL-*g*-HPC polymers using O-ATRP.

The LCSTs of the synthesized polymers were determined by assessing their transmittance as a function of temperature. We explored the impact of different pH conditions on LCST and successfully expanded the LCST range of HPC-based thermoresponsive polymers to align with physiological temperatures of 25–38 °C. Furthermore, we achieved a reverse pH dependency in LCST, providing enhanced versatility and control over these thermo-responsive polymers. The advancement of nonionic, thermo-responsive cellulose-based polymers with tunable properties across a broad range of physiological conditions offers promising applications in areas such as electronics, biosensors, cosmetics, textiles, and particularly in drug delivery systems.

2. Experimental section

2.1. Materials

Hydroxypropyl cellulose (HPC) was used with a molecular weight of 180 456 g mol^{-1}, as provided by Carbosynth, UK. *N*-Vinylcarpolactam (NVCL, 99.0%), 2-Bromopropionyl bromide (98%), hydrochloric acid (HCl, 37%), sodium hydroxide (NaOH, 99.2%) anhydrous dichloromethane (DCM, 99.8%), and dimethylformamide (DMF, 99.5%) were purchased from Sigma-Aldrich. While the photoredox catalyst 1,2,3,5-tetrakis(carbazol-9-yl)-4,6-dicyanobenzene (4CzIPN) was synthesized using our previous reported method.[30]

2.2. Synthesis of hydroxypropyl cellulose macroinitiator (HPC-I)

Prior to synthesizing stimuli-responsive polymers through O-ATRP, a macroinitiator was prepared following a previously reported method.[5,31] For this purpose, HPC (1.22 g) and DCM (140 mL) were stirred overnight to prepare a homogeneous solution. Subsequently, the reaction mixture was cooled to 5–10 °C using an ice bath, followed by the gradual addition of

2-bromopropionyl bromide (93 mg, 0.4 mmol) dissolved in 20 mL of anhydrous DCM. The mixture was then allowed to stir at ambient temperature (~25 °C) for 24 hours. Afterwards, the reaction mixture was allowed to stand for one hour, resulting in formation of precipitates which were separated by centrifugation (4000 rpm, Gf). The crude product underwent two washes with methanol and was then dried at 50 °C for a duration of 6 hours.

2.3. Synthesis of poly(*N*-vinylcarpolactam)-*g*-hydroxypropyl cellulose polymers

Three different polymers, denoted HNC-06, HNC-12, and HNC-18, were synthesized through visible light-driven O-ATRP, catalyzed by (Scheme 1). The polymers were different from each other in their compositions, as reflected by the varying molar ratios of HPC to NVCL. HNC-06, HNC-12, and HNC-18 were prepared with molar ratios of 94 : 06, 88 : 12, and 82 : 18 respectively, corresponding to the feeding ratio of HPC to NVCL utilized in the synthesis reaction. Identical synthetic procedures were employed for the preparation of all these three polymers, with the synthesis of HNC-18 serving as an illustrative example. A 225 mg of the macroinitiator was introduced into a dried glass reactor along with 2 mL of anhydrous DMF. Once the macroinitiator was fully dissolved in DMF, 2 mL of NVCL and 20 mg of 4CzIPN were added to the reaction mixture. Following the addition of the reagents, nitrogen gas was bubbled through the reaction mixture for 30 minutes to eliminate air. Then, the polymerization was initiated by exposing the reaction mixture to blue visible light for 12 hours at approximately 25–30 °C while maintaining a closed system. Subsequently, the polymer was isolated from the reaction mixture by precipitating it in 50 mL of methanol. The resulting solid was filtered off and then subjected to vacuum drying to remove any residual solvent and separate low molecular weight PNVCL residues.

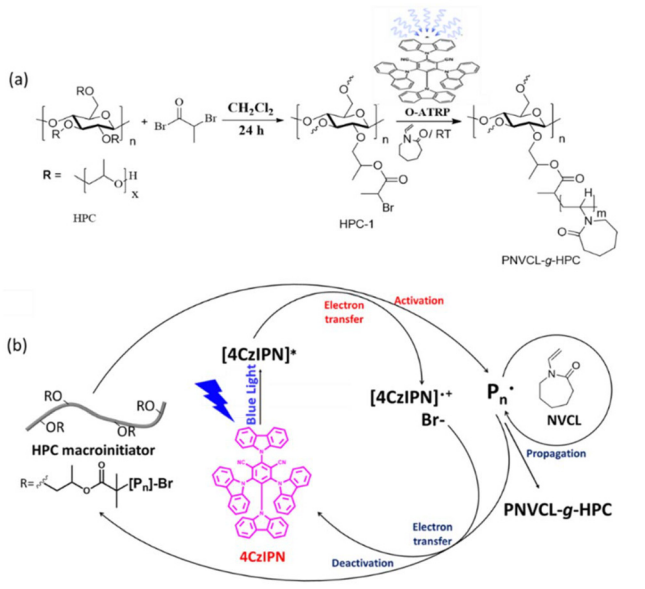

Scheme 1 (a) Preparation of PNVCL-*g*-HPCs polymer. (b) The O-ATRP mechanism.

2.4. Characterization

Fourier transform infrared (FT-IR) spectroscopy was used to characterize the chemical structure of HPC, macroinitiator (HPC-1) and the synthesized polymers using a Bruker Equinox 55 FT-IR spectrometer. The FT-IR spectra were acquired over a spectral range of 4000 to 400 cm^{-1}. To prepare the samples for analysis, potassium bromide (KBr) pellets were utilized. Proton nuclear magnetic resonance (^{1}H NMR) spectroscopy was employed to elucidate the molecular structure of the synthesized polymers using a Bruker ARX 400 MHz spectrometer operating at a frequency of 400 MHz. The NMR measurements were performed at a constant temperature of 25 °C, using chloroform-d_3 ($CDCl_3$) and deuterated dimethyl sulfoxide (DMSO-d_6) as suitable solvents for the macroinitiator and polymers, respectively. To analyze the molecular weight and dispersity index ($Đ$) of the synthesized polymers, gel permeation chromatography (GPC) was employed. The process involved using a 1200-series precision pump for sample delivery, a 1200-series diode array detector for concentration measurements, and a 1250-series evaporative light scattering detector for molecular weight analysis. Polymethyl methacrylate (PMMA) standards were employed to calibrate by Gel permeation Chromatographic system, ensuring accurate molecular weight measurements. A Mettler Toledo 822 thermogravimetric analyzer was used to assess the thermal stability of the polymers. The analysis was conducted with a continuous nitrogen atmosphere, heating the samples at a rate of 10 °C per minute from ambient temperature up to 600 °C. The lower critical solution temperatures (LCSTs) of the PNVCL-*g*-HPCs polymer samples were determined by the transmittance method. To explore the temperature-dependent characteristics of the HNC-06, HNC-12 and HNC-18 polymers, their aqueous solutions were analyzed for transmittance. This analysis was conducted at a concentration of 10 mg mL^{-1} using a UV/vis spectrophotometer (Shimadzu UV-2401PC) specifically measuring the transmittance at a wavelength of 550 nm. The pH values of the HNC-06, HNC-12 and HNC-18 aqueous solutions were modified by adding HCl and NaOH. The LCST is determined as the temperature where the transmittance reduces by 50%. UV/Vis spectrophotometer (Shimadzu UV-2401PC) was used to measure the optical densities (OD) of all polymer solutions at a concentration of 10 mg mL^{-1}. The assessments were carried out by gradually elevating the temperature from 25 °C to 65 °C, employing a heating rate of 10 °C min^{-1}. Measurements were taken at a wavelength of 550 nm throughout this temperature range. Dynamic light scattering (DLS) experiments were performed at a scattering angle of 90° using a commercial spectrometer (ALV/SP-150). Prior to measurement, the polymer solutions were filtered through a Millipore Millex-FH nylon filter (0.40 μm). The hydrodynamic radius (R_h) was calculated by fitting the correlation function using the CONTIN program. Each sample was equilibrated for 45 minutes at the specified temperature before analysis.

3. Results and discussion

3.1. Synthesis of macroinitiator (HPC-1)

Scheme 1(a and b) illustrates the preparation of HPC-1, the PNVCL-*g*-HPC polymers, and the O-ATRP mechanism. The initial step involved the preparation of a hydroxypropyl cellulose-based macroinitiator (HPC-1). This was achieved through esterification of the hydroxyl groups present on the cellulose backbone with 2-Bromopropionyl bromide. While in second step, this macroinitiator was used to graft NVCL monomers on cellulose backbone *via* O-ATRP using 4CzIPN as photoredox catalyst, resulting in the synthesis of PNVCL-*g*-HPCs polymers.

3.2. Synthesis of PNVCL-*g*-HPCs polymers

Three different polymers (HNC-06, HNC-12, and HNC-18) were synthesized using NVCL monomer and HPC-1 *via* O-ATRP (Scheme 1). During O-ATRP, the 4CzIPN catalyst absorbs blue light, transitioning to an excited state. The excited catalyst then participates in an oxidation process, reducing HPC-1 and producing a bromide anion, a propagating radical ($Pn^{\bullet}$), and a radical cation. The propagating radical subsequently initiates the polymerization process, leading to the formation of polymers.

After the initiation phase, polymer chains extend through the stepwise incorporation of monomers. Concurrently, a deactivation process converts the growing polymer chains into a dormant state, while also restoring the catalyst to its original form, thus completing the cycle of O-ATRP. The detailed mechanism underlying O-ATRP has been extensively explored and reported in the literature.[24,32,33]

3.3. Structural analysis of HPC-1 and polymers

The synthesis of HPC-1 and polymers was verified using a combination of analytical techniques, including FT-IR, ^{1}H NMR spectroscopy, TGA, and GPC.

3.3.1. FT-IR spectroscopy. The FT-IR spectrum of HPC-1 (Fig. 1b) shows a distinct peak at 1734 cm^{-1}, which is attributed to the ester carbonyl groups. This peak is not observed in the spectrum of HPC (Fig. 1a). Additionally, the broad peak associated with the hydroxyl groups of cellulose, was typically observed around 3400 cm^{-1}. Apart from this distinguishing feature, the remaining absorption bands of HPC-1 closely resemble those of HPC, indicating a high degree of similarity in their overall chemical composition. These FT-IR spectral changes provided evidence for the synthesis of cellulose based macroinitiator with ester functionalities.

The structure of the prepared polymers was also analyzed by FT-IR spectroscopy. Fig. 1(c) presents the spectrum of HNC-18 as a representative example. This spectrum revealed the presence of both the amide carbonyl group 1637 cm^{-1} and the carbonyl group of ester linkage at 1720 cm^{-1}. Notably, this amide carbonyl peak was absent in the FT-IR spectrum of HPC-1. While, both these peaks at 1637 and 1720 cm^{-1} were absent in HPC. The presence of these distinct peaks in the HNC-18 spectrum serves as evidence for the successful grafting of PNVCL chains onto the HPC surface. These findings align well with those reported in earlier studies.[5,34]

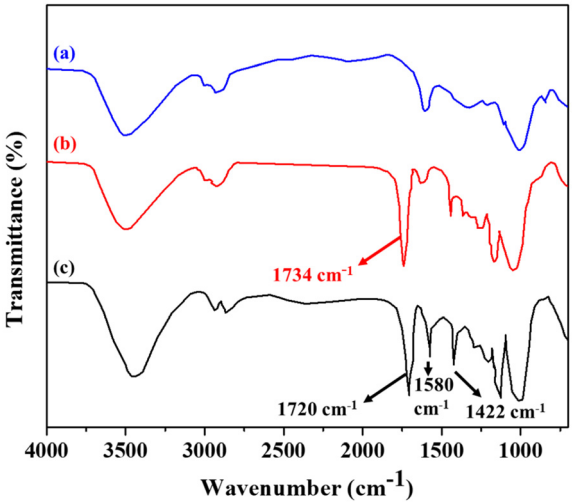

Fig. 1 FT-IR spectra of (a) HPC, (b) HPC-1, and (c) PNVCL-*g*-HPC.

3.3.2. NMR spectroscopy. The structures of HPC, HPC-1, and PNVCL-*g*-HPC polymers were further investigated using ^{1}H NMR spectroscopy (Fig. 2a–c). Fig. 2 (spectrum a) presents the ^{1}H NMR spectrum of HPC, where the resonance peak at 1.04 ppm (peak a) is attributed to the methyl group of propyloxy side chains in HPC. In the ^{1}H NMR spectrum of HPC-1 (spectrum b), a resonance peak at 1.15 ppm (peak a) can be attributed to the methyl groups of the propyloxy side chains.

Notably, the NMR spectrum of HPC-1 exhibits a broad resonance peak at 1.83 ppm (peak b) which confirms the successful attachment of the initiator to HPC. This signal is not present in the spectrum of HPC. Furthermore, the ^{1}H NMR spectrum of HPC-1 indicates a broad signal at 5.32 ppm (peak c), corresponding to methine protons. This peak is also not present in the spectrum of HPC. This spectrum provides

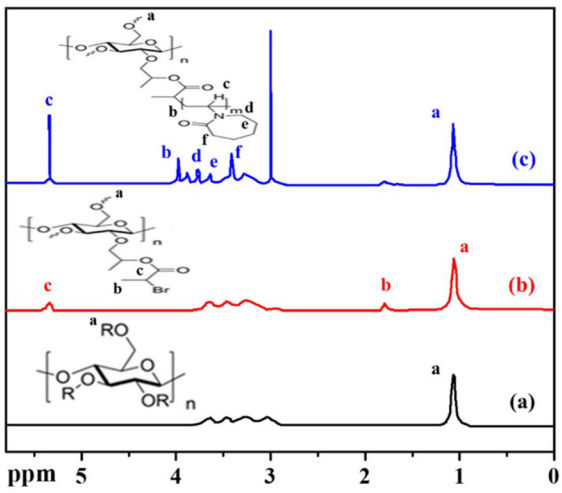

Fig. 2 ^{1}H NMR spectra of (a) HPC, (b) HPC-1, and (c) PNVCL-*g*-HPC.

further confirmation of the successful esterification of hydroxypropyl cellulose. These findings align with previously reported data in the literature, further validating the structure of HPC-1.[35,36]

Using ^{1}H NMR spectroscopy, the structural characteristics of the polymers were also investigated. Fig. 2 (spectrum c) depicts the ^{1}H NMR spectrum of HNC-18 as a representative example. In this spectrum, the peak at 1.1 ppm (peak a) is attributed to the methyl group protons of the HPC backbone, and this peak was also present in spectra a and b. In the spectrum of HNC-18, a resonance peak at 3.8 ppm (peak b) corresponds to the methylene group of the vinyl component, while a methine group appears at 5.3 ppm (peak c). Resonance peaks between 3.2–3.6 ppm (peaks d, e, and f) are associated with the methylene protons of the caprolactam ring. The distinct signals observed at positions b–f in the ^{1}H NMR spectrum of PNVCL-*g*-HPC can be attributed to the protons of the PNVCL side chains. This correlation between the ^{1}H NMR signals and the PNVCL structure provides further evidence of the successful grafting of PNVCL chains onto the HPC surface.

In summary, the combined results from FT-IR and ^{1}H NMR spectroscopy confirm the structural integrity of HPC, HPC-1, and the synthesized polymer (HNC-18), demonstrating the successful synthesis of the HNC-18 polymer.

3.4. Gel permeation chromatography (GPC)

The molecular weight and dispersity index ($Đ$) of HNC-06, HNC-12, HNC-18, and HPC were determined using GPC. The resulting chromatograms are presented in Fig. 3, while Table 1 summarizes the molecular weight and $Đ$ values. Notably, all the polymers exhibited a narrow $Đ$, with values of 1.4 for HNC-06, 1.3 for HNC-12, and 1.1 for HNC-18, even at higher molecular weights. These findings show the effectiveness of the O-ATRP technique in producing polymers with high molecular weight, a narrow $Đ$, and devoid of metal contamination.

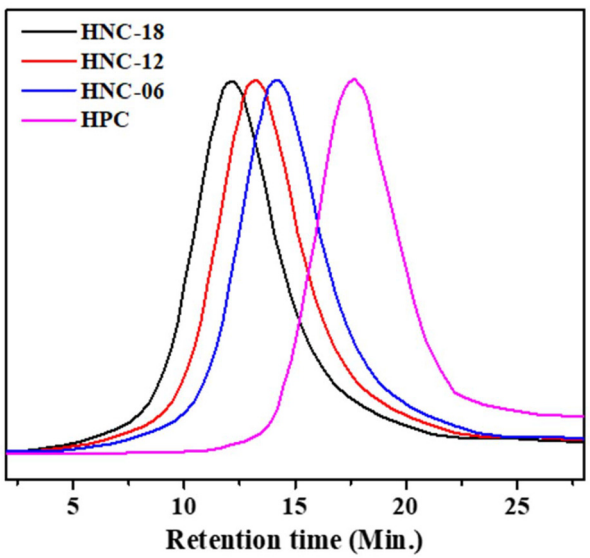

Fig. 3 GPC Chromatograms of HPC, HNC-06, HNC-12, and HNC-18 polymers.

Table 1 M_n, $Đ$, and V_h of HPC, HNC-06, HNC-12, and HNC-18 polymers

Sample	M_n (g mol^{-1})	($Đ$)	V_h (mL mol^{-1})
HPC	180 000	1.8	1.61×10^6
HNC-06	261 000	1.4	2.18×10^6
HNC-12	280 000	1.3	2.45×10^6
HNC-18	308 000	1.1	2.86×10^6

M_n = number average molecular weight, V_h = hydrodynamic volume, $Đ$ = polydispersity index.

Additionally, Mark–Houwink equation was used to determine the hydrodynamic volume (V_h) of HNC-06, HNC-12, and HNC-18, and HPC,[5] the obtained data is shown in Table 1. GPC analysis revealed that PNVCL-*g*-HPCs polymers possess a higher hydrodynamic volume than HPC. Furthermore, a positive correlation was observed between the hydrodynamic volume of PNVCL-*g*-HPC and the molecular weight of polymers.

3.5. Investigation of polymerization kinetics

GPC analysis was employed to investigate polymerization kinetics, with HNC-18 serving as the model system for kinetic studies. The semilogarithmic plot in Fig. 4 depicts the conversion of monomer as a function of time. The initial monomer concentration is denoted by M_0, while M_t represents the monomer concentration at a specific time. A linear relationship is observed in the plot of $\ln([M]_0/[M]_t)$ *vs.* time in Fig. 4(a), particularly during the initial phase of polymerization up to approximately six hours. This linear trend suggests that first-order kinetics govern the polymerization process during this time frame.[37,38] Beyond the initial linear phase, the graph in Fig. 4(a) exhibits a slight curvature, suggesting a shift away from the previously linear trend. This shift might be due to factors such as the use of a polar solvent like DMF or reduced radical concentration, resulting in termination of active free radicals.[39,40]

Fig. 4(b) depicts the correlation between the ($Đ$) and M_n of PNVCL side chains, which were produced by hydrolyzing PNVCL-*g*-HPC, as a function of monomer conversion. The

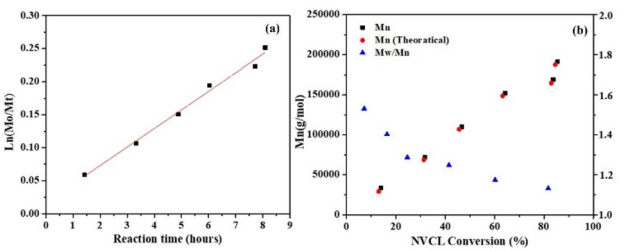

Fig. 4 (a) Semilogarithmic kinetic plot of consumption of monomer *versus* polymerization time. (b) Changes in $Đ$ (M_w/M_n) and M_n of NVCL side chains with respect to monomer conversion.

molecular weights of these PNVCL chains exhibited a linear relationship with monomer conversion, indicating a controlled polymerization process. Fig. 4(b) further illustrates that the molecular weights of the polymers obtained from GPC measurements closely matched the theoretical values. This further confirms that the polymerization was well-controlled and living.[5]

3.6. Thermogravimetric analysis

The thermal characteristics of HPC, HPC-1, PNVCL, HNC-06, HNC-12, and HNC-18 were assessed through thermogravimetric analysis. Fig. 5 displays the thermograms for these materials, while Table 2 presents data on thermal stability, including T_5, T_{10}, T_{50}, and R_{600}. The TGA thermogram reveals that HPC undergoes a one-step degradation process with a T_{50} value of 365 °C. In contrast, HPC-1 exhibits reduced thermal stability (T_{50} = 329 °C) compared to HPC. This decreased thermal stability of HPC-1 is attributed to the presence of bromoalkyl groups, which release hydrogen bromide upon heating during TGA analysis.[35,41] In the case of PNVCL-*g*-HPC polymers, the thermal degradation of HNC-18 manifests as a two-stage process. The initial weight loss, occurring around 100 °C, is likely due to the removal of residual moisture. The first stage of degradation occurs between 358 °C and 414 °C, while the second stage initiates at approximately 482 °C and persists until 503 °C. Significantly, HNC-18 has a T_{50} value of 503 °C, surpassing the T_{50} values observed for HPC and HPC-1. This enhanced thermal stability can be primarily attributed to the chain extension that occurs during the synthesis of the final polymer. Additionally, HNC-18 also shows a higher R_{600} value compared to HPC and HPC-1. The thermal stabilities of HNC-06 and HNC-12, as observed in Fig. 5, exhibit a similar pattern.

As a control experiment, we assessed the thermal stability of the homopolymer *N*-vinyl caprolactam (PNVCL). As shown in Table 2 and Fig. 5, PNVCL exhibited a T_{50} value of 438 °C with a multistep degradation pattern, which differs from those observed for HPC, HPC-1, HNC-06, HNC-12, and HNC-18.

Thus, HNC-06, HNC-12, and HNC-18 have higher T_{50} values than HPC and HPC-1. These results reveal that HNC-06, HNC-12, and HNC-18 polymers have been successfully synthesized, exhibiting a different thermal stability compared to HPC and HPC-1.

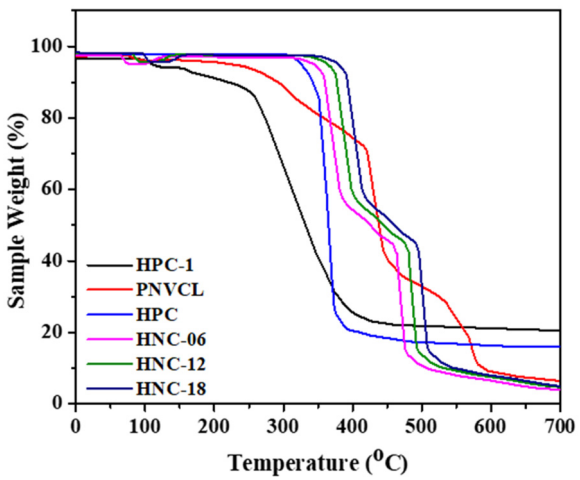

Fig. 5 TGA of HPC, HPC-1, PNVCL, HNC-06, HNC-12, HNC-18 polymers.

Table 2 TGA analysis of HPC, HPC-1, HNC-06, HNC-12, and HNC-18

Samples	T_5 (°C)	T_{10} (°C)	T_{50} (°C)	R_{600} (%)
HPC	325	343	365	16.2
HPC-1	112	213	329	21.6
PNVCL	221	296	438	6.2
HNC-06	344	361	470	6.4
HNC-12	364	378	485	6.9
HNC-18	388	392	503	7.8

T_5, T_{10}, and T_{50} are the temperatures at which 5%, 10%, and 50% weight loss occur. R_{600} displays the residual mass at 600 °C.

3.7. Investigation of pH- and thermo-responsive behavior

The pH- and thermo-responsive behavior of HPC, HNC-06, HNC-12, and HNC-18 polymers in an aqueous solution was determined by exploring their LCSTs. The LCSTs of these polymers were investigated using the transmittance method. In Fig. 6(a), we present the changes in transmittance observed in the HNC-18 aqueous solution when subjected to variations in temperature and pH. Meanwhile, Fig. 6(b) highlights the relationship between pH and LCST. Fig. 6(a) illustrates a decrease in the LCST of HNC-18 with rising pH levels. Additionally, the polymer solutions exhibited a reduction in transmittance to around 55% and 25% at pH values of 3.0 and 4.5, respectively (Fig. 6a), some polymer chains have the ability to self-assemble, which explains this behavior.[5] PNVCL is

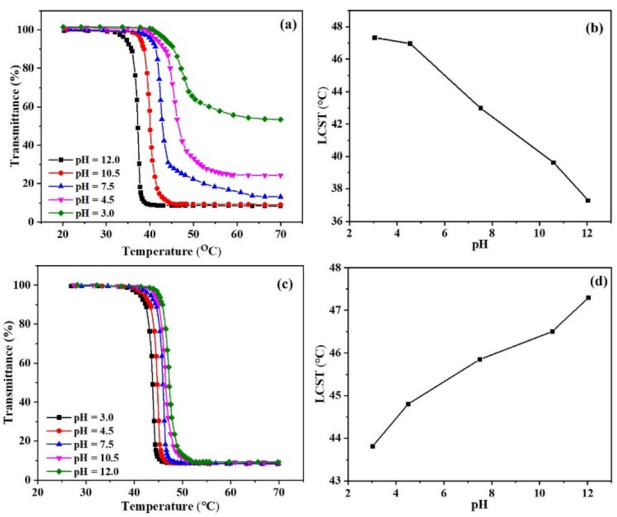

Fig. 6 (a and c) Temperature-dependent transmittance of HNC-18 and HPC at different pH levels, (b and d) LCST of HNC-18 and HPC plotted against different pH values.

acknowledged for its propensity to undergo protonation when exposed to an acidic solution. This protonation effect elevates electrostatic repulsion, consequently hindering the process of phase separation.[42,43] Likewise, as shown in Fig. 6(b), it is evident that the LCST decreased from 47.3 to 37.2 °C as the pH of the solution was increased from 3.0 to 12.0, attributable to the grafting of PNVCL chains onto HPC. These outcomes highlight the direct correlation between the LCST of HNC-18 and the pH of the polymer solution. Consequently, the HNC-18 polymer exhibited dual pH and temperature-responsive characteristics in aqueous environments. These findings align well with earlier research in this area.[44–46] In order to assess the properties of the polymers, we investigated how the LCST of HPC responded to variations in both temperature and pH, as depicted in Fig. 6(c and d). As Fig. 6(d) clearly illustrates, an elevation in pH led to an increase in the LCST for HPC, in contrast to HNC-18, where LCST increases by increasing pH. This behavior can be attributed to the disruption of hydrogen bonds between HPC and water molecules.[47] Similarly, the reason behind the lower LCST of HNC-18 when compared to HPC can be traced to the formation of hydrogen bonds between HPC (hydrogen bond donor) and PNVCL (acting as hydrogen bond acceptors). These results signify that the biocompatible HNC-18, which responds to dual stimuli, possesses an LCST of 37.2 °C, well-aligned with the physiological temperature range of 25–38 °C. Consequently, HNC-18 exhibits considerable potential for a wide array of applications, including biomedical engineering, biosensors, drug delivery system.

Similar findings were observed for HNC-06 and HNC-12, as illustrated in Fig. 7, where an increase in pH led to a reduction in the LCST of these polymers. Fig. 7 demonstrates that at a pH of 12.0, the LCST values were 41.5 °C for HNC-06 and 39.4 °C for HNC-12.

Fig. 8 indicates the changes in hydrodynamic radius (R_h) of HNC-18 with temperature at various pH values. Dynamic Light Scattering (DLS) experiments were used to measure the hydrodynamic radius of the polymers. For this purpose, an aqueous solution of HNC-18 polymer with a concentration of 2 mg mL^{-1} was used to measure R_h. Fig. 8 shows that at a pH of 3.0, the initial R_h value did not change significantly when the temperature was raised from 25 °C to around 43 °C. After that, the R_h value gradually increased. The same trend was observed at pH values of 4.5, 7.5, 10.5, and 12.0, where the R_h value initially remained almost the same and then increased sharply. This sharp increase in R_h was observed at temperatures of 42, 40, 39, and 37 °C at pH values of 4.5, 7.5, 10.5, and 12.0, respectively. Interestingly, both R_h and LCST showed similar responses to changes in pH and temperature, indicating that these two properties are complementary.

Fig. 9 presents the optical densities of HPC, HNC-06, HNC-12, and HNC-18 polymers, recorded at 550 nm while

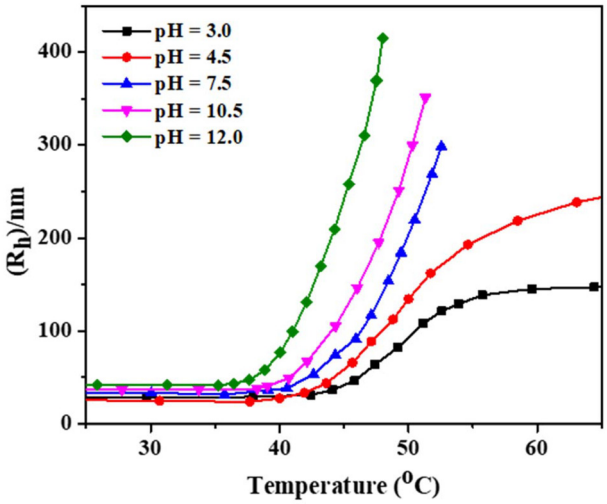

Fig. 8 Variations in hydrodynamic radius (R_h) of HNC-18 in an aqueous solution with temperature and pH.

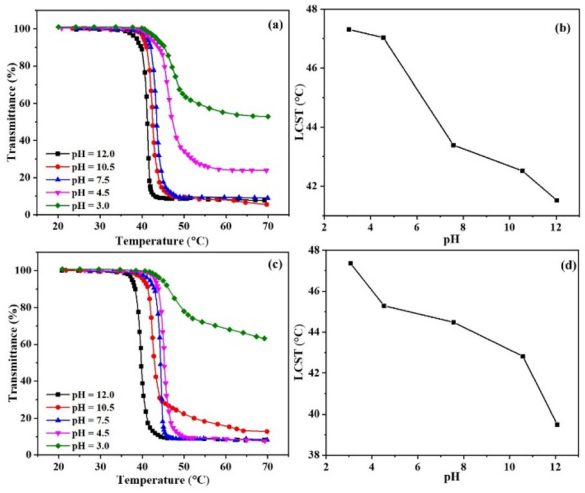

Fig. 7 (a and c) HNC-06 and HNC-12 transmittance as a function of temperature at various pH levels. The LCST of HNC-06 and HNC-12 in relation to pH is shown in (b and d).

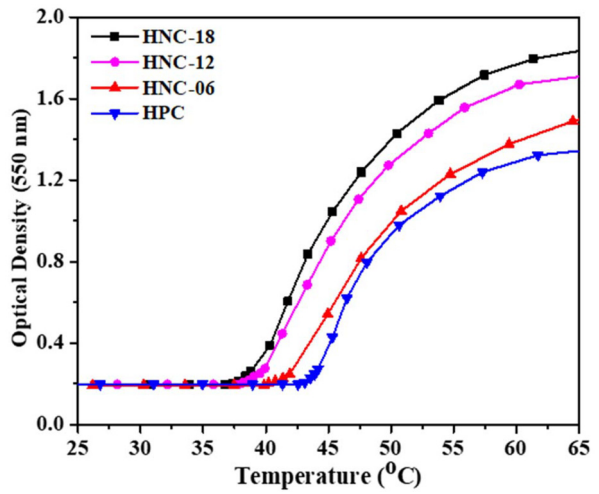

Fig. 9 Optical density of HPC, HNC-06, HNC-12 and HNC-18 polymers in an aqueous solution.

their aqueous solutions were heated from 25 to 65 °C. HPC shows very small value of optical density, around 0.188, from 25 to 43.8 °C, indicating maximum solubility in water within this temperature range. This behavior is because HPC exhibits LCST behavior in water. Below its LCST, HPC is typically soluble in water, forming a homogeneous solution. However, by increasing the temperature from 43.8 to 65 °C, HPC becomes insoluble, and its optical density increases from 0.188 to 1.3. When the temperature surpasses the LCST of HPC, the polymer chains undergo a phase transition, leading to the formation of a separate phase, often appearing as cloudy or gel-like precipitates in the solution. The reason for this phase separation is that the interactions between the polymer and the water molecules alter considerably above the LCST, causing the HPC molecules to preferentially interact with each other rather than staying dispersed in the water.[5]

For HNC-06, the optical density remained consistent at 0.87 until reaching 41.5 °C, beyond which it escalated to 1.4 at 65 °C. This observed shift suggests that heating the solution beyond 41.5 °C prompts the polymer to exhibit a tendency to form aggregates. This behavior is attributed to the presence of PNVCL segments within the polymer, serving as hydrophobic components in an aqueous solution, leading to aggregation.

At 65 °C, HNC-12 demonstrated an optical density of 1.58, maintaining a consistent value of 0.185 between 25 and 39.4 °C. Similarly, HNC-18 indicated an optical density of 0.87 from 25 to 37.2 °C, which increased as the temperature rose from 37.2 to 65 °C, reaching a value of 1.8 at 65 °C. However, above their LCST, HNC-06, HNC-12, and HNC-18 polymers became insoluble and formed aggregates due to the hydrophobic PNVCL segments, finally undergoing a phase transition.

The increased optical density at elevated temperatures is due to the dehydration of HPC components, which enhances hydrophobic interactions between the PNVCL segments. As the temperature increases, water molecules bound to the hydrophilic groups in HPC are expelled, resulting in a loss of solubility. The dehydrated HPC segments expose their hydrophobic core, triggering the aggregation of polymer chains. PNVCL, a thermoresponsive polymer, undergoes an LCST transition, where above the LCST, the PNVCL segments become hydrophobic, leading to phase separation and aggregation. This aggregation enhances the hydrophobic interactions between the polymer chains, contributing to the observed increase in optical density. These results align well with the previous studies.[15,48–51]

Finally, increasing the contents of hydrophobic PNVCL segments in HNC-06, HNC-12, and HNC-18 resulted in two observed trends. The first trend was an increased optical density of the polymers, due to enhanced self-association and light scattering at higher temperatures caused by the aggregation of PNVCL domains. The second trend was a reduction in LCST, implying a weakened interaction between the water molecules and polymer due to the presence of hydrophobic PNVCL segments. Additionally, the data clearly demonstrate a strong relationship between the optical density and the thermoresponsive properties of the polymers.

In the present work, the thermosensitive behavior of PNVCL-*g*-HPC polymers is tuned by varying the polymer concentration. The effect of polymer concentration in an aqueous solution on thermoresponsive behavior is investigated using HNC-18 polymer concentrations ranging from 2.0 to 9.5 mg mL^{-1}. To calculate the LCST, light transmittance at 550 nm is measured as a function of temperature (Fig. 10). Consistent with expectations, the LCST of HNC-18 was observed to decrease from 37.8 °C to 35.2 °C as the polymer concentration rose from 2.0 to 9.5 mg mL^{-1}, indicating a concentration-dependent change in LCST. This trend illustrates how the phase transition temperature of HNC-18 in aqueous solutions diminishes with increasing polymer concentration, aligning with established principles of LCST behavior in dilute solutions as documented in prior studies.[16,48,52] This principle suggests that at lower polymer concentrations, strong hydrogen-bonding interactions between water molecules and polymer chains are promoted. In this case, more thermal energy is required to break the hydrogen bonds, leading to an increase in LCST. However, at higher polymer concentrations, weaker hydrogen-bonding interactions between water molecules and polymer chains are promoted. Consequently, less thermal energy is required to disrupt the hydrogen bonds, ultimately leading to a decrease in LCST. These results are consistent with previous studies.[52,53]

The thermosensitive behavior of PNVCL-*g*-HPC polymer was also tuned by varying the length of the hydrophobic PNVCL block chain. Fig. 11 illustrates how the molecular weight of the PNVCL block influences the LCST. The LCST values were found to be approximately 42 °C, 39 °C, and 37 °C for HNC-06, HNC-12, and HNC-18, respectively. Given that PNVCL is inherently hydrophobic, the PNVCL-*g*-HPC polymers exhibit reduced hydrophilicity compared to the HPC homopolymer. Consequently, the HNC-18 polymer, which has a longer

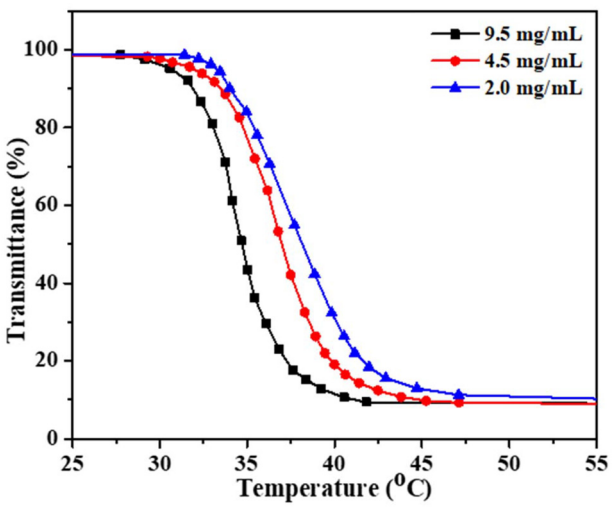

Fig. 10 The effect of concentration of PNVCL-*g*-HPC polymer on LCST.

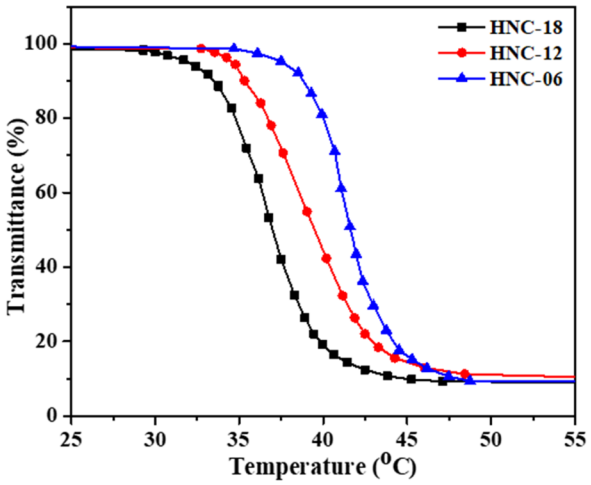

Fig. 11 Influence of block length and balance between hydrophobic and hydrophilic segments on the LCST for HNC-06, HNC-12, and HNC-18 polymers.

PNVCL segment, shows lower hydrophilicity than HNC-06 and HNC-12, resulting in lower LCST values, as anticipated.[54]

In HNC-18, HPC behaves as a hydrophilic polymer in aqueous solution at temperatures below its LCST, meaning it is soluble in water and interacts favorably with water molecules. At temperatures above its LCST, HPC becomes hydrophobic or water-insoluble because the hydrogen bonds between the HPC chains and water molecules become less stable at higher temperatures, causing the HPC chains to aggregate. The hydrophilicity of HPC is due to hydrogen bonding with water molecules, which helps to keep the HPC chains dispersed in water. The hydrophobicity of HPC at temperatures above its LCST is due to the weakening of these hydrogen bonds, resulting in aggregation.[16,55]

PNVCL is a polymer that can exhibit both hydrophilic and hydrophobic properties depending on temperature. It contains hydrophilic amide groups and hydrophobic carbon–carbon backbones. At temperatures below its LCST, PNVCL tends to be hydrophilic, meaning it has an affinity for water and can dissolve or swell in aqueous solutions. However, as the temperature increases beyond the LCST, the polymer undergoes a phase transition and becomes hydrophobic, repelling water and losing its solubility in aqueous solutions. Thus, hydrophobic behavior dominates compared to its hydrophilic behavior.

Similarly, the HNC-12 polymer, with a longer PNVCL block length than HNC-06, is less hydrophilic, resulting in a lower LCST value. These findings are consistent with earlier research.[16,56–58] This observation suggests that by adjusting the balance between hydrophilicity and hydrophobicity, it is possible to regulate the phase transition temperature of these polymers to fit within the desired range. This property is often exploited in various applications, including food additives, pharmaceuticals, cosmetics, and especially biomedical applications to control the release of drugs.

4. Conclusions

This study successfully synthesized and characterized dual pH- and thermo-responsive PNVCL-*g*-HPC polymers using metal-free, visible-light-driven organocatalyzed atom transfer radical polymerization (O-ATRP) with 4CzIPN as the photoredox catalyst. Comprehensive analyses, including FT-IR, NMR, TGA, and GPC, validated the high quality and successful synthesis of these polymers. We addressed the challenge of high LCST in HPC-based polymers by tuning the composition ratios of HPC and PNVCL monomers, achieving precise control over the LCST. Specifically, the LCST of the HNC-18 polymer was reduced from 43.8 °C to 37.2 °C as pH increased from 3.0 to 12.0. This reduction in LCST demonstrates the effectiveness of our approach and the potential of PNVCL-*g*-HPC polymers for applications requiring precise thermal responsiveness. The ability to tailor the LCST of these polymers opens new opportunities for their use in various advanced fields, including electronics, biosensors, pharmaceuticals, biomedical engineering, and drug delivery systems. The efficiency and versatility of the synthesized polymers underscore their promise for diverse technological applications.

Author contributions

Conceptualization, Toheed Akhter and Muhammad Asif Iqbal; methodology, Muhammad Asif Iqbal; validation, Toheed Akhter and Sadaf Ul Hassan; formal analysis, Muhammad Asif Iqbal; investigation, Muhammad Asif Iqbal; resources, Toheed Akhter, Chan Ho Park, Asif Mahmood, and Waheed Al-Masry; writing – original draft preparation, Toheed Akhter and Sadaf Ul Hassan; writing – review and editing, Toheed Akhter and Chan Ho Park; supervision, Toheed Akhter. All authors have read and agreed to the published version of the manuscript.

Data availability

All data supporting the findings of this study are included within the manuscript.

Conflicts of interest

The authors declare that there are no conflicts of interest.

Acknowledgements

The authors acknowledge the funding provided by Researcher's Supporting Project Number (RSP2024R43), King Saud University, Riyadh, Saudi Arabia. This work was also supported by the National Research Foundation of Korea (NRF) grant funded by the Korea government (MSIT) (No. RS-2024-00408370).

References

1 S. J. Lugger, S. J. Houben, Y. Foelen, M. G. Debije, A. P. Schenning and D. J. Mulder, *Chem. Rev.*, 2021, **122**, 4946–4975.
2 X. Yan, F. Wang, B. Zheng and F. Huang, *Chem. Soc. Rev.*, 2012, **41**, 6042–6065.
3 J. M. Korde and B. Kandasubramanian, *Ind. Eng. Chem. Res.*, 2019, **58**, 9709–9757.
4 H. Ullah, H. A. Santos and T. Khan, *Cellulose*, 2016, **23**, 2291–2314.
5 M. A. Iqbal, T. Akhter, M. Faheem, A. Mahmood, W. Al-Masry, S. Nadeem, S. U. Hassan and C. H. Park, *Cellulose*, 2023, **30**, 7519–7533.
6 H. C. Arca, L. I. Mosquera-Giraldo, V. Bi, D. Xu, L. S. Taylor and K. J. Edgar, *Biomacromolecules*, 2018, **19**, 2351–2376.
7 K. A. Heitfeld, T. Guo, G. Yang and D. W. Schaefer, *Mater. Sci. Eng., C*, 2008, **28**, 374–379.
8 M. Gosecki, H. Setälä, T. Virtanen and A. J. Ryan, *Carbohydr. Polym.*, 2021, **251**, 117015.
9 S. Graham, P. F. Marina and A. Blencowe, *Carbohydr. Polym.*, 2019, **207**, 143–159.
10 P. Khuman, W. B. K. Singh, S. D. Devi and H. Naorem, *J. Macromol. Sci., Part A: Pure Appl.Chem.*, 2014, **51**, 924–930.
11 X. Xia, S. Tang, X. Lu and Z. Hu, *Macromolecules*, 2003, **36**, 3695–3698.
12 H. Kang, R. Liu and Y. Huang, *Polymer*, 2015, **70**, A1–A16.
13 L. Marsili, M. Dal Bo, G. Eisele, I. Donati, F. Berti and G. J. P. Toffoli, *Polymers*, 2021, **13**, 2639.
14 M. N. Mohammed, K. B. Yusoh and J. H. B. H. Shariffuddin, *Mater. Express*, 2018, **8**, 21–34.
15 N. A. Cortez-Lemus and A. Licea-Claverie, *Prog. Polym. Sci.*, 2016, **53**, 1–51.
16 R. M. Moraes, L. T. Carvalho, G. M. Alves, S. F. Medeiros, E. Bourgeat-Lami and A. M. Santos, *Polymers*, 2020, **12**, 1252.
17 S. Medeiros, A. Santos, H. Fessi and A. Elaissari, *Int. J. Pharm.*, 2011, **403**, 139–161.
18 A. Kumar, S. Sharma, S. Afgan, R. Kumar, A. K. Keshari and R. Srivastava, *Int. J. Biol. Macromol.*, 2018, **112**, 780–787.
19 K. Parkatzidis, H. S. Wang, N. P. Truong and A. Anastasaki, *Chem*, 2020, **6**, 1575–1588.
20 M. Chen, M. Zhong and J. A. Johnson, *Chem. Rev.*, 2016, **116**, 10167–10211.
21 C.-W. Tu, F.-C. Tsai, C.-J. Chang, C.-H. Yang, S.-W. Kuo, J. Zhang, T. Chen and C.-F. Huang, *Polymers*, 2019, **11**, 1631.
22 F. Lorandi, M. Fantin and K. Matyjaszewski, *J. Am. Chem. Soc.*, 2022, **144**, 15413–15430.
23 M. Kumar, P. S. Gehlot, D. Parihar, P. K. Surolia and G. Prasad, *Eur. Polym. J.*, 2021, **152**, 110448.
24 V. K. Singh, C. Yu, S. Badgujar, Y. Kim, Y. Kwon, D. Kim, J. Lee, T. Akhter, G. Thangavel and L. S. Park, *Nat. Catal.*, 2018, **1**, 794–804.
25 P. R. Rodrigues and R. P. Vieira, *Eur. Polym. J.*, 2019, **115**, 45–58.
26 D. J. Siegwart, J. K. Oh and K. Matyjaszewski, *Prog. Polym. Sci.*, 2012, **37**, 18–37.
27 G. Szczepaniak, J. Piątkowski, W. Nogaś, F. Lorandi, S. S. Yerneni, M. Fantin, A. Ruszczyńska, A. E. Enciso, E. Bulska and K. Grela, *Chem. Sci.*, 2020, **11**, 4251–4262.
28 D. A. Corbin and G. M. Miyake, *Chem. Rev.*, 2021, **122**, 1830–1874.
29 J. C. Theriot, B. G. McCarthy, C. H. Lim and G. M. Miyake, *Macromol. Rapid Commun.*, 2017, **38**, 1700040.
30 V. K. Singh, C. Yu, S. Badgujar, Y. Kim, Y. Kwon, D. Kim, J. Lee, T. Akhter, G. Thangavel and L. S. C. Park, *Nat. Catal.*, 2018, **1**, 794–804.
31 L.-l. Yang, J.-m. Zhang, J.-s. He, J. Zhang and Z.-h. Gan, *Chin. J. Polym. Sci.*, 2015, **33**, 1640–1649.
32 D. A. Corbin and G. M. Miyake, *Chem. Rev.*, 2021, **122**, 1830–1874.
33 S. de Ávila Gonçalves, P. R. Rodrigues and R. Pioli Vieira, *Macromol. Rapid Commun.*, 2021, **42**, 2100221.
34 B. Gautam and H.-h. Yu, *Polymers*, 2020, **12**, 2920.
35 M. Bagheri and L. Pourmirzaei, *Macromol. Res.*, 2013, **21**, 801–808.
36 T. A. Debele, S. L. Mekuria, S.-Y. Lin and H.-C. Tsai, *RSC Adv.*, 2016, **6**, 14692–14704.
37 M. Hurtgen, J. Liu, A. Debuigne, C. Jerome and C. Detrembleur, *J. Polym. Sci., Part A: Polym. Chem.*, 2012, **50**, 400–408.
38 Z. Yu, J. Yi and D. Tang, *Sep. Purif. Technol.*, 2020, **249**, 116888.
39 S. F. Medeiros, M. V. Lopes, B. Rossi-Bergmann, M. I. Ré and A. M. Santos, *Drug Dev. Ind. Pharm.*, 2017, **43**, 1519–1529.
40 M. Andrei, P. O. Stănescu, C. Drăghici, L. M. Butac and M. Teodorescu, *Colloid Polym. Sci.*, 2018, **296**, 1905–1915.
41 S. Deng, S. Binauld, G. Mangiante, J. Frances, A. Charlot, J. Bernard, X. Zhou and E. Fleury, *Carbohydr. Polym.*, 2016, **151**, 899–906.
42 X. Qi, X. Tong, W. Pan, Q. Zeng, S. You and J. Shen, *J. Cleaner Prod.*, 2021, **315**, 128221.
43 L. Marsili, M. Dal Bo, F. Berti and G. Toffoli, *Pharmaceutics*, 2021, **13**, 1654.
44 L. Ma, R. Liu, J. Tan, D. Wang, X. Jin, H. Kang, M. Wu and Y. Huang, *Langmuir*, 2010, **26**, 8697–8703.
45 Z. Li and M. Zhang, *Polymers*, 2023, **15**, 3643.
46 L. Ma, H. Kang, R. Liu and Y. Huang, *Langmuir*, 2010, **26**, 18519–18525.
47 Y. R. Lee, D. Park, S. K. Choi, M. Kim, H. S. Baek, J. Nam, C. B. Chung, C. O. Osuji and J. W. Kim, *ACS Appl. Mater. Interfaces*, 2017, **9**, 31095–31101.
48 K. M. Rao, K. S. V. K. Rao and C.-S. Ha, *Gels*, 2016, **2**, 6.
49 S. Durkut and Y. M. Elçin, *Macromol. Chem. Phys.*, 2020, **221**, 1900412.
50 N. S. Rejinold, T. Baby, K. Chennazhi and R. Jayakumar, *J. Biomed. Nanotechnol.*, 2015, **11**, 392–402.
51 A. Lu, E. Petit, S. Li, Y. Wang, F. Su and S. Monge, *Int. J. Biol. Macromol.*, 2019, **135**, 38–45.
52 J. Peng, D. Tang, H. Lv, N. Wang, X. Yang, Z. Sun and Z. Yu, *Colloid Polym. Sci.*, 2019, **297**, 1255–1264.

53 R. Liu, T. Ding, P. Deng, X. Yan, F. Xiong, J. Chen and Z. Wu, *Int. J. Biol. Macromol.*, 2022, **194**, 358–365.
54 Y. Yang, J. Li, M. Hu, L. Chen and Y. Bi, *J. Polym. Res.*, 2014, **21**, 1–9.
55 K. Kumar, R. Umapathi, K. Ramesh, S.-K. Hwang, K. T. Lim, Y. S. Huh and P. Venkatesu, *Langmuir*, 2021, **37**, 1682–1696.
56 Q. Wu, L. Wang, X. Fu, X. Song, Q. Yang and G. Zhang, *Polym. Bull.*, 2014, **71**, 1–18.
57 H. Vihola, A. Laukkanen, L. Valtola, H. Tenhu and J. Hirvonen, *Biomaterials*, 2005, **26**, 3055–3064.
58 M. Sta, G. Aguiar, A. A. Forni, S. F. Medeiros, A. M. Santos and N. R. Demarquette, *J. Appl. Polym. Sci.*, 2020, **137**, 48472.